Charge photo-carrier transport from silicon nanocrystals embedded in SiO 2 -based multilayer structures

B. Dridi Rezgui, F. Gourbilleau, D. Maestre, Olivier Palais, A. Sibai, M. Lemiti, G. Brémond

Charge photo-carrier transport from silicon nanocrystals embedded in SiO_2-based multilayer structures

B. Dridi Rezgui,[1,3,a)] F. Gourbilleau,[2] D. Maestre,[3] O. Palais,[3] A. Sibai,[1] M. Lemiti,[1] and G. Brémond[1]
[1]*Université de Lyon, Institut des Nanotechnologies de Lyon INL-UMR 5270, CNRS, INSA de Lyon Bât. Blaise Pascal, 7 av. Jean Capelle, Villeurbanne F-69621, France*
[2]*CIMAP, UMR CEA/CNRS/Ensicaen/UCBN, 6 Boulevard Maréchal Juin, 14050 Caen Cedex 4, France*
[3]*Aix-Marseille Univ. and CNRS, IM2NP, IM2NP, Faculté des Sciences de Jérome, F-13397 Marseille France*

(Received 5 February 2012; accepted 20 June 2012; published online 30 July 2012)

Experimental investigation of photoconductivity in Si-rich silicon oxide (SRSO)/SiO_2 multilayer (ML) structures prepared by magnetron reactive sputtering is reported. Photocurrent (PC) measurements show that the PC threshold increases with decreasing the thickness of SRSO layer. Photo-conduction processes in our samples are shown to be dominated by carrier transport through quantum-confined silicon nanocrystals embedded in the SiO_2 host. In addition, the observed bias-dependence of photocurrent intensity is consistent with a model in which carrier transport occurs by both tunneling and hopping through defect states in the silicon oxide matrix. A photocurrent density J_{ph} of 1–2 mA cm^{-2} is extracted from our results. Although this photocurrent density along the ML absorber film is relatively low, the results presented in this work are believed to be a valuable contribution toward the implementation of all-Si tandem solar cells. © *2012 American Institute of Physics*. [http://dx.doi.org/10.1063/1.4737579]

I. INTRODUCTION

Silicon nanocrystals (Si NCs) are a fascinating area of science and one that has significant technological implications. Such nanostructures have been extensively studied in the last decade for high efficiency light emission, which hold promise for some innovative applications in photonics based on silicon technology.[1–3] More recently, it has been proposed to take advantage of the quantum confinement effect in Si NC for photovoltaic applications by managing the silicon bandgap and consequently producing efficient tandem solar cells.[4,5] Different technological approaches allowing formation of such Si nanostructures have already been developed either in silicon-rich dielectric layer[6–8] or in multilayer (ML) structure.[9–11] It has been reported the advantage of such nanostructure to tune the energy band gap of Si NC in the appropriate range (1.7–1.8 eV) which is required to maximize conversion efficiency.[12] Among these approaches, SiO_2-based nanometric multilayer structures attract considerable interest since they allow managing the silicon grain size in the Si-rich sublayer for an optimization of the carrier transport.[13] Such features indicate that compositional periodic Si-rich silicon oxide (SRSO)/SiO_2 multilayer system may be a promising structure for "third generation" photovoltaic applications.[14] Previous studies of these structures focused on structural and optical properties have been reported elsewhere[15–18] but a lack of quantitative measurements of photogenerated current persists.

Photocurrent (PC) spectroscopy is one of the important tools for the opto-electrical characterization of semiconductor materials.[19,20] The generation of photocurrent can be divided into three steps: (i) the absorption of optical energy and generation of carriers, (ii) the transport of photogenerated carriers, and (iii) the collection of the carriers at the electrodes. The movement of carriers gives rise to the photocurrent, which persists until both electrons and holes are collected at the electrodes or until they recombine in the material before reaching their respective electrodes. This measurement provides an idea about the electronic properties (optical bandgap) of the material as well as its intrinsic transport features. The photocurrent equation is given by[21]

$$I_{ph} \propto \frac{I_0}{\hbar\omega}\left[(1-\exp(-\alpha d)) - \frac{\alpha L\left(1-\exp\left(-d\left(\alpha+\frac{1}{L}\right)\right)\right)}{\left(1+\frac{\tau_{sr}}{\tau_b}\right)(1+\alpha L)}\right], \quad (1)$$

where I_{ph} is the photocurrent at a particular energy, α is the absorption coefficient at that energy, I_0 is the impinging light intensity on the surface, $I_0/\hbar\omega$ is the photon flux, L is the light penetration depth, d is the film thickness, and τ_{sr}/τ_b is the ratio of surface to the bulk recombination time. This equation describes the proportionality between I_{ph} and the absorbance minus loss due to surface recombination.

Recently, it has been shown that a high density of Si NCs, close to 10^{19} cm^{-3}, in such multilayer systems can be reached.[15] In addition, absorption coefficient was found to be dependent on the nanocrystal size.[16] The higher concentration of Si NCs would be advantageous for the carrier photoconductivity and therefore the solar cell performance. In this paper, the opto-electrical properties of SRSO/SiO_2 multilayer structures prepared by magnetron reactive sputtering method are studied. In particular, the PC dependence on the grain size and on the applied bias is investigated. We demonstrate the improvement of the photocurrent response through

a)Electronic mail: bechir.rezgui@im2np.fr.

the bias voltage control. Finally, the current density in the multilayers was evaluated under equivalent photon flux of the AM1.5 solar spectrum.

II. EXPERIMENTAL DETAILS

Multilayer structures based on silicon oxide were deposited by reactive magnetron sputtering on a p-type (100)-oriented silicon substrate at 500 °C. The ML growth process which alternates the deposition of stoichiometric SiO_2 followed by SRSO layer consists in sputtering a pure SiO_2 target with hydrogen-rich plasma for incorporating Si excess in the growing layer. The thickness of SRSO layer (t_{SRSO}), and consequently the Si grain size, was controlled by adjusting the deposition time. The power density applied for the sputtering of the SiO_2 target was 0.76 W cm^{-2}, whereas the hydrogen and argon partial pressures were fixed at 6.0 and 1.5 Pa, respectively. Four SRSO/SiO_2 multilayer structures, referred as ML1, ML2, ML3, and ML4, were prepared under the same conditions and distinguished only by the thickness of the active SRSO layer and, therefore, the size of Si NCs. More details of the fabrication process can be found elsewhere.[16] After deposition, the samples were annealed at 1100 °C during 1 h under N_2 atmosphere in order to assure the good Si/SiO_2 phase separation. Detailed characteristics of the different ML films are listed in Table I. In order to perform lateral PC measurements, the transmission line model (TLM) pattern, consisting of Al isolated square contacts separated by variable distances, was fabricated. A post-metallization annealing at 500 °C during 15 h under N_2 atmosphere was performed in order to improve the contact resistances. Photocurrent spectra were measured with lock-in technique by exciting the sample surface with chopped (110 Hz) light. The sample was irradiated with a 150 W halogen lamp, whose emission was monochromatically dispersed by means of a Jobin-Yvon HR640 monochromator. The photogenerated current was collected by a current amplifier (Keithley 428) and the biases were applied using a Keithley 2410 voltage source. Before exciting the sample, the monochromatic light passed through a long pass filter, in order to eliminate higher order diffraction replica, and through a chopper wheel, which provided the lock-in reference frequency. The schematic diagram of the experimental setup used for our PC measurement is shown in Fig. 1. The PC spectra have been corrected with a calibrated pyroelectric optical detector. In addition, room-temperature photoluminescence (RT-PL) analyses were carried out using the 458 nm line from an Ar^+ ion laser source. The emission was detected with a Jobin-Yvon iHR320 spectrometer coupled to a liquid-nitrogen-cooled CCD Hamamatsu camera.

TABLE I. Characteristics of the investigated SRSO/SiO_2 multilayer films.

Sample	t_{SiO2} (nm)	t_{SRSO} (nm)	Number of bilayers
ML1	1.5	8	3
ML2	1.5	6	11
ML3	1.5	3	7
ML4	1.5	1.5	5

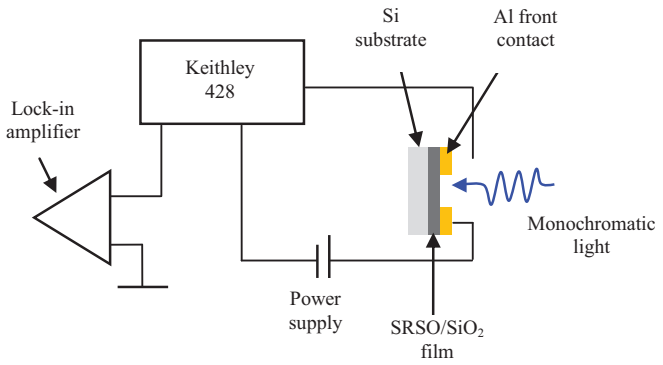

FIG. 1. Schematic diagram of lateral photocurrent measurements.

III. RESULTS AND DISCUSSION

To investigate the absorption characteristics, photocurrent measurements were carried out for each of the multilayers. Fig. 2 shows the spectral dependence of lateral photocurrent of the ML films measured at 300 K and at bias voltage of −2 V. As can be observed in the figure, the photocurrent signal starts from photon energy close to the band-gap of silicon. Therefore, we can assign the PC threshold around 1.05 eV to the crystalline silicon which could be explained by the diffusion of aluminum through the ML film to the substrate as illustrated in the inset of Fig. 2. More importantly, our experiments reveal two photocurrent edges which can be clearly observed in sample ML4 in the photon energy range between 1.05 and 1.4 eV. Furthermore, the PC maximum is shifted towards higher energy region when the grain's size is reduced from 8 nm to 1.5 nm. This variation of photocurrent peak position is mainly caused by the change of electronic energy levels in Si NCs due to the quantum confinement effect. The light absorption in the active SRSO layer which corresponds to the electronic transition between quantized energy levels in Si NCs could explain the second PC edge in ML4. Accompanying the blueshift in the PC maximum, the broadening of the photocurrent peak is a signature of the increase of the size distribution of Si NCs. It

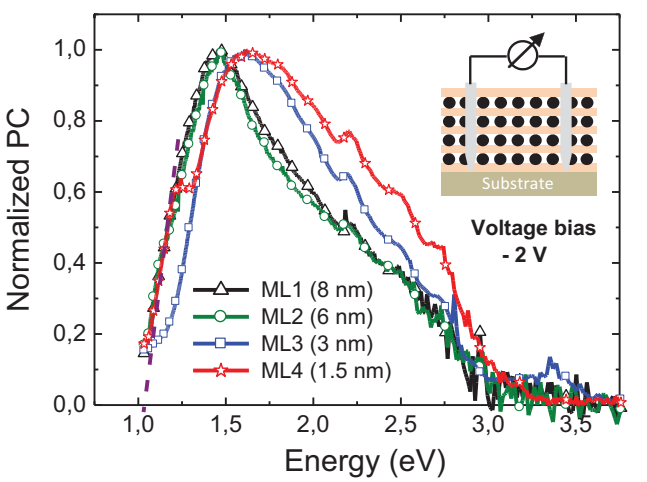

FIG. 2. Normalized photocurrent spectra of SRSO/SiO_2 multilayers versus energy. Inset: schematic of the sample structure for lateral photocurrent measurements.

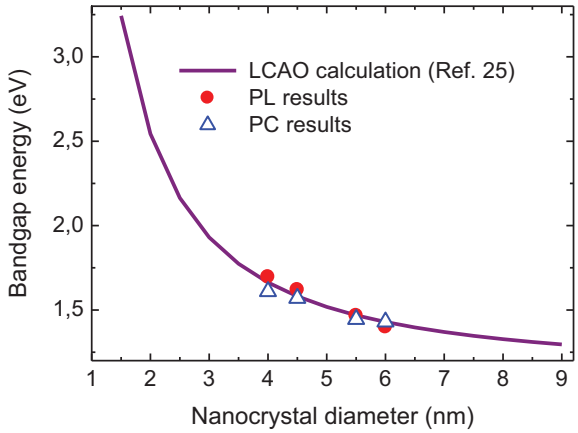

FIG. 3. Correlation between nanocrystal diameter, PL (closed circles) and PC (open triangles) peak energies. The experimental data points compare nicely with theoretical results obtained from linear combination of atomic orbitals (LCAO) calculation[25] (solid curve).

could also reflect the effect of the vibronic coupling between the electronic states in silicon nanocrystals and the SiO_2 matrix on the photocurrent response. This phenomenon has been interpreted well in Ref. 22. Considering the high density of Si NCs of $\sim 10^{19}\,cm^{-3}$, which was previously measured using transmission electron microscopy, the nanocrystal spacing was estimated to be about 1 nm.[15] This distance between Si NCs is small enough compared to the tunneling thickness predicted for silicon oxide embedded with silicon nanoparticles.[23] This process of carrier tunneling is consistent with the relatively strong coupling between the adjacent Si NCs.[24]

The dependence of the photocurrent threshold on the grain size is evidenced by photoluminescence (PL) measurement performed at room temperature. The variation of the bandgap energy obtained from PL and the maximum of PC peaks versus the nanocrystal diameter is shown in Fig. 3. As can be seen in this figure, our results are in good agreement with theoretical data.[25] The peak energy is shifted towards higher energies (with respect to bulk silicon) according to an inverse power law with an exponent of 1.39 (the solid curve in Fig. 3).

Fig. 4 depicts the room-temperature lateral photocurrent spectra of the multilayer films measured under different applied bias voltages. A very weak photocurrent signals (<20 pA) was observed at zero bias pointing to the fact that the films possess an intrinsic potential which is probably due to the nonuniformity of SRSO layer. The spectra show a rapid increase in PC signal with both negative and positive bias voltages due to the enhancement of the free photocarrier generation and transport. Significantly, an enhanced photocurrent was measured at negative bias in particular for ML2 and ML4 films. It should be noted that no photocurrent peak shift is observed with bias voltages. It is well known that the external field not only helps the free photocarrier generation but also enhances the photocarrier hopping by increasing the tunneling probability. Therefore, the observed PC in our ML films could be assigned to the contribution of both tunneling effect and hopping through defect states in the dielectric matrix.[26] Moreover, it can be seen in Fig. 4(d) that the photocurrent peak below the photon energy of 1.4 eV becomes more and more distinguishable with the increasing applied voltage bias.

Fig. 5 illustrates the extracted photocurrent intensity at the maximum of the PC peak as a function of the bias voltage. The I_{PC}-V curves present a linear behavior which gives reasons to believe that the current passing in the active SRSO layer is due to the tunneling mechanism.[27] The carriers preferentially move along the nanocrystalline silicon

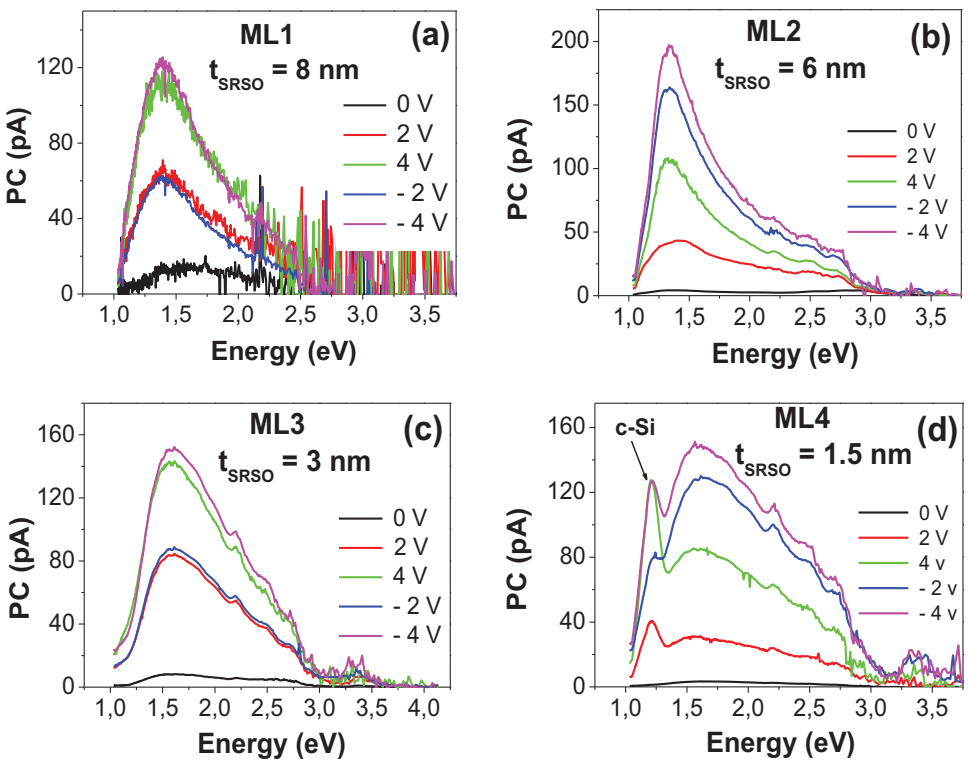

FIG. 4. Photocurrent spectra of SRSO/SiO_2 multilayers versus energy, for different positive and negative voltage biases.

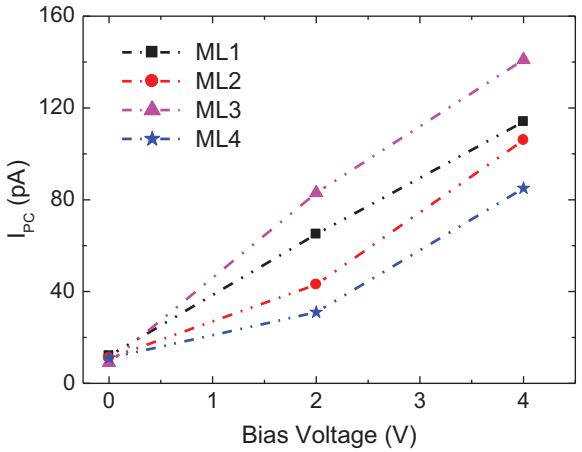

FIG. 5. Room-temperature photocurrent intensity versus bias voltage for different SRSO/SiO_2 multilayers

chains in the active SRSO layer and tunnel through the a-SiO_2 matrix, which separates the neighbouring nanocrystals. When the voltage is increased, thin oxide barriers between neighbouring nanocrystals are tunneled and the current increases quasi-linearly. However, carrier tunneling through defects in the dielectric host matrix cannot be excluded in such systems.[28]

Fig. 6(a) shows the PC spectra of ML3 sample versus energy, measured at a voltage bias of −2 V and temperature ranging from 13 to 300 K. Similar features were obtained for the other samples which contain smaller and bigger Si NCs. As expected, the overall structure of the photocurrent spectrum is shifted toward high energy as the sample is cooled down to 13 K. This shift is due to the temperature-dependent bandgap change which occurs in most semiconducting materials. Fig. 6(b) displays the variation of the bandgap energy extracted from PC measurements as a function of temperature on the ML3 sample. The temperature dependence of the bandgap energy in our experiment is well fitted by using the Varshni equation,[29]

$$E_g(T) = E_g(0) - \frac{\alpha T^2}{(T+\beta)}, \tag{2}$$

where α and β are parameters known as the Varshni thermal coefficient and the Debye coefficient, respectively. $E_g(0)$ is the bandgap energy at 0 K which is estimated to be 1.73 eV. When α and β are taken to be 9.63×10^{-4} eV/K and 336 K, respectively, the curve plotted by Eq. (2) closely fits the experimental values. The temperature dependency of the bandgap of silicon nanocrystals shows the same characteristic features as those in the crystalline silicon. In multilayer system, the carrier transport is governed by the potential barrier due to the thin silicon dioxide interlayer between Si NCs. In addition, the transport is generally determined by the competition between two main mechanisms depending on the temperature regimes: thermal activation and tunneling through the potential barrier. At high temperatures, carriers acquire the activation energy E_{act} necessary to overcome the potential barrier and the photogenerated current is due to the thermionic emission from Si NCs. As the temperature decreases, the probability of the thermal activation for the carriers localized in Si NCs is very low and tunneling through the potential barrier becomes the only possible mechanism of the transport.

One of the important physical parameters that need to be known for future photovoltaic applications is the photocurrent density J_{ph} produced in the nanostructured films. Therefore, to demonstrate the performance of such a structure for wide bandgap absorber layer in tandem solar cells, the light intensity was calibrated using a pyroelectric detector to produce a photocurrent equivalent to that obtained under AM1.5 (100 mW cm^{-2}) illumination. A photocurrent density of 1–2 mA cm^{-2} has been extrapolated for the investigated ML films. Although the structures studied in this work show a relatively small photocurrent values, a photovoltaic effect related to the presence of Si NCs is clearly observed. Moreover, it has been reported that the tunneling probability for a square potential well is given by[30]

$$T_e = 16 \exp\left\{-d\sqrt{\frac{8m^*}{\hbar^2}\Delta E}\right\}, \tag{3}$$

where m^* is the bulk effective mass in the respective band of the matrix, d is the spacing between nanocrystals and ΔE is the energy difference between the conduction band edge of the matrix and the confined energy level of the nanocrystals. Hence, transport between nanocrystals can be significantly

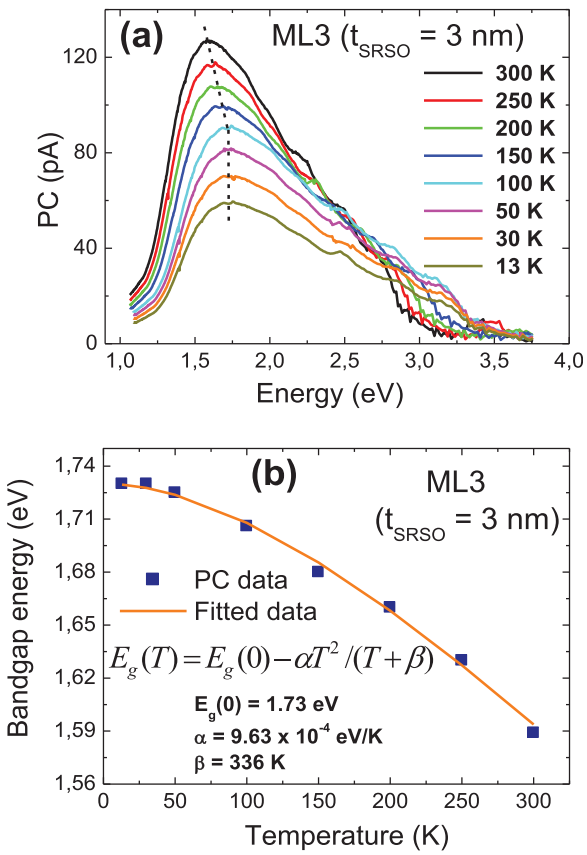

FIG. 6. (a) Plot of the photocurrent spectra of ML3 sample versus energy for temperatures varying from 13 to 300 K. (b) Variation of the bandgap energy (extracted from PC measurement) versus temperature for ML3 sample. The solid line is the fitting curve using the Varshni equation.

increased by the adoption of another dielectric matrix with smaller barrier height such as silicon nitride or silicon carbide in silicon-based multilayer structures.

IV. CONCLUSION

In conclusion, the nanocrystal size and voltage bias-dependent photogenerated current in SRSO/SiO_2 multilayer structures containing high density silicon nanocrystals were studied by photocurrent spectroscopy. The strong dependence of the PC threshold on the nanocrystal size was attributed to tunneling processes through Si NCs. This is clearly confirmed by the observed blueshift of the photoluminescence peak energy due to the confinement effect related to the decreased size of Si NCs. The effect of the voltage bias on the photocurrent of different multilayers was also investigated. The carrier transport in our samples is believed to be governed by tunneling conduction via Si NCs and hopping transport through defect states in the silicon oxide matrix. The photocurrent density extracted from the multilayer films show a promising but not sufficient values paving the way to a successful application of such absorber material in all-silicon tandem solar cells.

ACKNOWLEDGMENTS

This work was supported by the French National Agency for Research (ANR) through the DUOSIL project. Financial support has also been partly funded by the Rhône-Alpes region in the frame of the PHOSIL project.

[1]N. Lalic and J. Linnros, J. Lumin. **80**, 263 (1999).
[2]S.-H. Choi, and R. G. Elliman, App. Phys. Lett. **75**, 968 (1999).
[3]B.-H. Kim, C.-H. Cho, T.-W. Kim, N.-M. Park, G. Y. Sung, and S.-J. Park, Appl. Phys. Lett. **86**, 091908 (2005).
[4]E.-C. Cho, M. A. Green, G. Conibeer, D. Song, Y.-H. Cho, G. Scardera, S. Huang, S. Park, X. J. Hao, Y. Huang, and L. V. Dao, Adv. OptoElectron. **2007**, 1 (2007).
[5]J. De la Torre, G. Bremond, M. Lemiti, G. Guillot, P. Mur, and N. Buffet, Mater. Sci. Eng. C **26**, 427 (2006).
[6]B. Rezgui, A. Sibai, T. Nychyporuk, M. Lemiti, G. Bremond, D. Maestre, and O. Palais, Appl. Phys. Lett. **96**, 183105 (2010).
[7]L. Ding, T. P. Chen, Y. Liu, C. Y. Ng, and S. Fung, Phys. Rev. B **72**, 125419 (2005).
[8]L. V. Mercaldo, E. M. Esposito, P. D. Veneri, B. Rezgui, A. Sibai, and G. Bremond, J. Appl. Phys. **109**, 093512 (2011).
[9]G. Scardera, T. Puzzer, I. Perez-Wurfl, and G. Conibeer, J. Cryst. Growth **310**, 3680 (2008).
[10]F. Gourbilleau, C. Dufour, B. Rezgui, and G. Bremond, Mater. Sci. Eng. B **159**, 70 (2009).
[11]D. Song, E.-C. Cho, G. Conibeer, Y. Huang, C. Flynn, and M. A. Green, J. Appl. Phys. **103**, 083544 (2008).
[12]N.-M. Park, T.-S. Kim, and S.-J. Park, App. Phys. Lett. **78**, 2575 (2001).
[13]M. Zacharias, J. Heitmann, R. Scholtz, U. Kahlere, M. Schmidt, and J. Blasing, Appl. Phys. Lett. **80**, 661 (2002).
[14]M. A. Green, *Third Generation Photovoltaics: Ultra-High Efficiency at Low Cost* (Springer-Verlag, Berlin, 2003).
[15]D. Maestre, O. Palais, D. Barakel, M. Pasquinelli, C. Alfonso, F. Gourbilleau, M. De Laurentis, and A. Irace, J. Appl. Phys. **107**, 064321 (2010).
[16]F. Gourbilleau, C. Ternon, D. Maestre, O. Palais, and C. Dufour, J. Appl. Phys. **106**, 013501 (2009).
[17]C. Ternon, F. Gourbilleau, X. Portier, P. Voivenel, and C. Dufour, Thin Solid Films **419**, 5 (2002).
[18]X. J. Hao, E.-C. Cho, C. Flynn, Y. S. Shen, G. Conibeer, and M. A. Green, Nanotechnology **19**, 424019 (2008).
[19]K. P. Acharya, H. Khatri, and B. Ullrich, J. Appl. Phys. **105**, 103111 (2009).
[20]B. Ullrich and A. Erlacher, J. Phys. D: Appl. Phys. **38**, 4048 (2005).
[21]A. Erlacher, M. Ambrico, V. Capozzi, V. Augelli, H. Jaeger, and B. Ullrich, Semicond. Sci. Technol. **19**, 1322 (2004).
[22]C. Xu, Z. P. Li, W. Pan, and W. Z. Shen, Appl. Surf. Sci. **257**, 8409 (2011).
[23]M. A. Green, E.-C. Cho, Y. Cho, Y. Huang, E. Pink, T. Trupke, A. Lin, T. Fangsuwannarak, T. Puzzer, G. Conibeer, and R. Corkish, in 20th European Photovoltaic Solar Energy Conference, 6–10 June 2005, Barcelona, Spain, pp. 3–7.
[24]S. Gardelis, P. Manousiadis, and A. G. Nassiopoulou, Nanoscale Res. Lett. **6**, 227 (2011).
[25]C. Delerue, G. Allan, and M. Lannoo, Phys. Rev. B **48**, 11024 (1993).
[26]C.-W. Jiang, M. A. Green, E.-C. Cho, and G. Conibeer, J. Appl. Phys. **96**, 5006 (2004.)
[27]I. Stavarache, Dig. J. Nanomater. Biostruct. **6**, 1073 (2011).
[28]C.-W. Jiang, M. A. Green, E.-C. Cho, and G. Conibeer, J. Appl. Phys. **96**, 5006 (2004).
[29]Y. P. Varshni, Physica **34**, 149 (1967).
[30]K. Boer, *Survey of Semiconductor Physics*, van Nostrand Reinhold, 1990.